

A CALIBRATION APPROACH FOR THE FULLY POLARIMETRIC AIRBORNE C BAND MICROWAVE RADIOMETER: THEORETICAL BASIS AND FIRST FIELD RESULTS.

Hanh Pham, The University of Michigan, Ann Arbor, MI (hpham@umich.edu)
Mentor: Dr. Edward Kim, NASA GSFC, Code 975

Abstract. *The Airborne C band Microwave Radiometer (ACMR) is an additive analog polarimeter and represents GSFC's first attempt to build a fully polarimetric microwave radiometer. A "black box" approach was adopted to calibrate the instrument. For such an instrument, knowledge of magnitude and phase imbalances is more critical than for a "standard" single or dual polarized radiometer because of the need to combine the V polarized and H polarized signals. Therefore, extensive laboratory measurements of ACMR were carried out and results were imported into a theoretical model describing the signals in their entirety through the radiometer, including various non-ideal properties. An elegant first order approximation inversion allows retrieval of the full modified Stokes vector, and the first calibrated field results of the 7th Radiobrightness and Energy Balance Experiment (REBEX7) are obtained.*

INTRODUCTION

Polarization of the reflected and scattered radiation adds a new dimension to the measurement and understanding of the remote sensing radiated field. The motivation of this calibration work is twofold. Concerning the scientific purpose, polarimetric signatures draw an increasing interest for ocean wind speed retrieval (Piepmeier,2001). Polarimetry also shows potential in remote sensing of soil moisture, snow, vegetation and polarimeters will help modelers to assimilate their polarimetric emission signatures. Concerning the engineering purpose, calibration feed back can lead to better future design and construction.

To express the polarimetric characteristics of an electromagnetic wave, we can use the modified Stokes vector:

$$\bar{T}_B = \begin{pmatrix} T_V \\ T_H \\ T_{45^\circ} - T_{-45^\circ} \\ T_l - T_r \end{pmatrix} = \frac{\lambda^2}{k_B \eta} \begin{pmatrix} \langle |E_V|^2 \rangle \\ \langle |E_H|^2 \rangle \\ 2 \cdot \text{Re} \langle E_V \cdot E_H^* \rangle \\ 2 \cdot \text{Im} \langle E_V \cdot E_H^* \rangle \end{pmatrix}$$

The ultimate goal of this work is to deliver reliable modified Stokes parameters to scientists, the output information as seen by the end user being the output voltages appearing on the user-interface.

The Airborne C band Microwave Radiometer (ACMR) is a dual polarized radiometer with analog additive circuit. It underwent several hardware modifications between field experiments and parts of it come from other instruments prototypes. Because of the lack or lost of accurate exhaustive documentation, and the reluctance to dismount the instrument, a "black box" approach is adopted to calibrate the instrument. For a fully polarimetric instrument, knowledge of magnitude and phase imbalances are critical because of the back end analog combination of the Vpol and Hpol signals. Basically, the instrument can be decomposed in 4 stages:

- the antenna, followed by an orthomode transducer
- the remote receiver module including calibration switches and first stage amplification and filtering

- the polarimetric combining circuit featuring an electromechanical switch
- the local receiver module, a gain chain with a square law detector diode

The back end analog/digital converter assembly with a direct display on the computer screen won't be studied in this project. ACMR's calibration processes began back in 1997. Previous works included mainly: (1) 1997 :microwave measurement of parts of the receiver that are no longer in use in ACMR, or that have been modified afterwards, by A. W. Brooks Jr. (2) In 2000 : Yuka Muto in ACMR participation to REBEX7 in Michigan with antenna measurements by Steve Seufert ; (3) In 2001 : Anja Imig produced polarimetric circuit characterization (with Tom Dod, Code 555), end to end gain measurement, antenna pattern plots, and antenna efficiency measurement with cryoload technique.

These works present valuable engineering features, however they exhibit deficiencies such as: semi inconsistent antenna patterns, no VSWR data for the antenna, no characterization for the receiver used during REBEX7, end to end gain measurements omitting switching features, no switch repeatability test, no modified Stokes parameters delivered. The latter lack makes the ACMR unusable to the scientific community.

The ultimate goal of these work is to deliver usable data for the scientist to obtain an end to end gain, receiver noise calibration aka as radiometer calibration; a polarimetric transfer function, which can be obtained by determining the possible radiometer non idealities such as channel unbalances (different mismatches, gains...), cross talk/contamination between polarizations, and leakage from the signal coming from antenna.

APPROACH

The « black box » is the most intuitive approach to calibrate ACMR within a restrained amount of time, since we are not expressly interested in the inner workings of the system. Let us consider a quasi-monochromatic wave incident on the antenna. A transition occurs through the antenna, transforming the unguided wave into a voltage at the V and H port. We'll define an antenna transfer function transforming unguided wave into voltages at the antenna ports, and transfer functions describing the Remote Receiver Module and Polarimetric Circuit behaviors. These three quantities can be derived from laboratory measurements that yield respectively antenna patterns in the anechoic chamber, several S parameters using a Vector Network Analyzer. Figure 1 shows a system level block diagram with the measurable quantity at each stage, and induced transfer functions.

Since the Polarimetric Circuit has a *single* output describing the amplitude of the combined signal for left, right, +45° and -45° polarization and of the modified vertical and horizontal polarization, there is no more phase imbalances or magnitude imbalance issues. The configuration is equivalent to that of a single receiver. Therefore, no S parameter measurement is needed. Only gain and noise knowledge of the combined {Local Receiver Module and Analog to Digital Converter } are desired. These latter parameters are included in the end to end characterization of the ACMR, as we read directly the digitized detected amplified low voltage on the computer interface screen.

From this approach, we can derive a polarimetric transfer function as a combination of the signals entire behaviors through the system, and an end to end calibration regardless of the polarization. This latter calibration consists in a classic calibration as describe in [1]

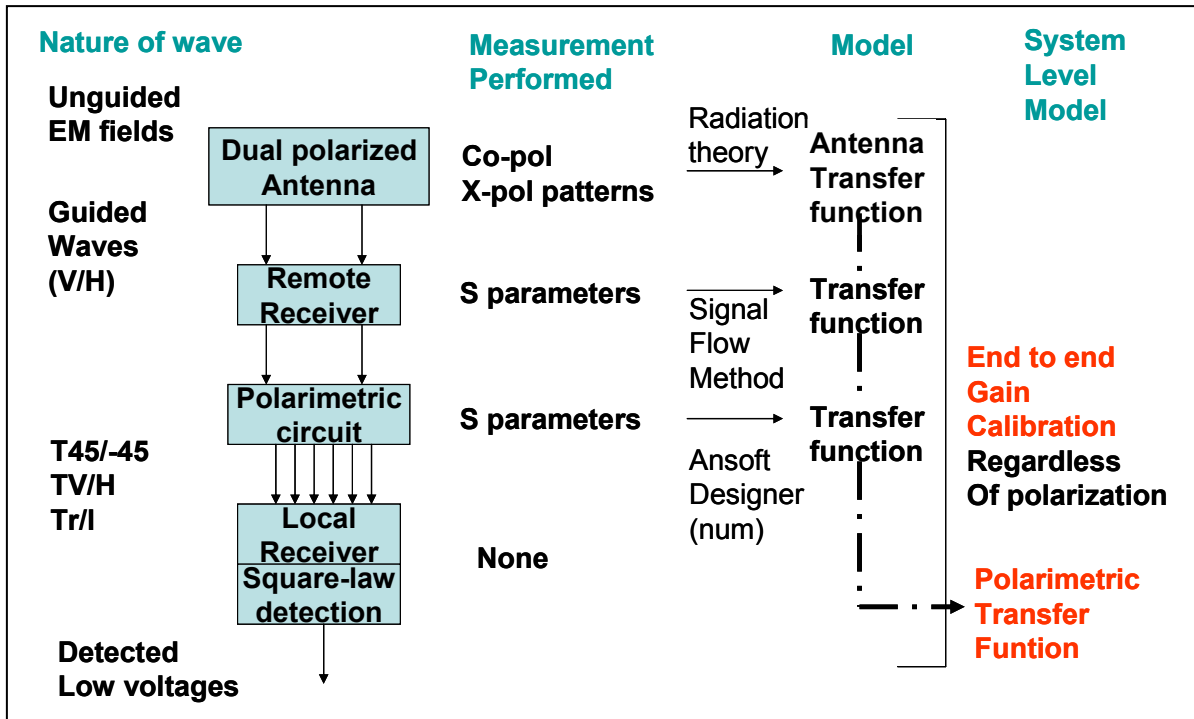


Figure 1. System level block diagram

Polarimetric transfer function

The ACMR antenna is a C band circular corrugated horn antenna with a plani-convex lens over the horn aperture combined with the associated orthomode transducer (OMT) interfacing SMA female ports. The antenna was designed and built by Microwave

Engineering Corporation, North Andover, Massachusetts, under the model 6351, S/N :695. It is centered at 6.925GHz, and features a HPBW of 300MHz. The antenna is linearly polarized. A picture of the antenna in the anechoic chamber in 2000 is displayed in Figure 2.

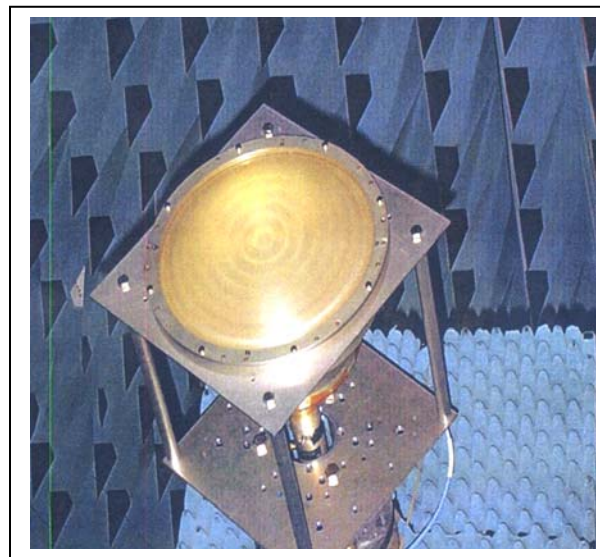


Figure 2. ACMR antenna in GSFC tapered range anechoic chamber

Tests were carried out in Spring 2000, using the data acquisition software GAAMS

x1.12. They include vv, vh, hh, hv raw data (Rx.Tx) at three frequencies :

h-h-675b-conv	h-v-675b-conv	v-h-675b-conv	v-v-675b-conv
h-h-6925b-conv	h-v-6925b-conv	v-h-6925b-conv	v-v-6925b-conv
h-h-7100b-conv	h-v-7100b-conv	v-h-7100b-conv	v-v-7100b-conv

where AUT is the receiver and the feed horn the transmitter. During summer 2001, Anja Imig wrote a set of Matlab code yielding copol and X pol patterns. Ohmic efficiency was also obtained during the same period [2]. Since the copol and X pol patterns present some inconsistencies, we decided to perform another set of measurements to see if any of the inconsistencies come from mechanical settings.

During summer 2003, measurements were performed [3]. Pieces of absorber were added to the antenna pillars in order to minimize reflections. Definitions of Copol and X pol are conform to Ludwig's 3rd definition [4]. The ACMR was the transmitting antenna at the end of the anechoic chamber, and can rotate its head around its boresight (0 to 180deg, with 2 deg increment), and rotate in azimuth around the stand axis (-180 to 180deg, with 1 deg increment). A Standard Feed Horn antenna could receive both Vertical and Horizontal polarizations at the same time. Data was obtained for V and H excitation separately

and 3 frequencies. Figure 3 illustrate the spatial coordinate system used.

The following points are obtained : **(1)** Differential phase between V and H output ports for V or H input polarization at several frequencies over the radiometer passband. 3 D map obtained with Matlab. Correspondence between raw data files and converted files are described in help files: convert_step1.xls, what's what.xls. Fig 4. shows the differential phase between V and H polarization of ACMR when it is transmitting V and H with no phase difference initially, for different observation points in space. The antenna is positioned in coordinates (0,0,0). If the antenna were perfect, since the offset distance between the input ports is $\lambda/2$, the differential phase should be 180 deg, and a perfect sphere of radius 180deg would appear on the plots. **(2)** Rectangular, polar, spherical magnitude and phase plots of co pol and X pol patterns for each linear polarizations obtained with GAAMS2. Applicable GAAMS2 file: cal to sgh- acmr--6-19-03.ant. A PC GAAMS2 viewer is available. A sample of these plots is showed in Figure 5.

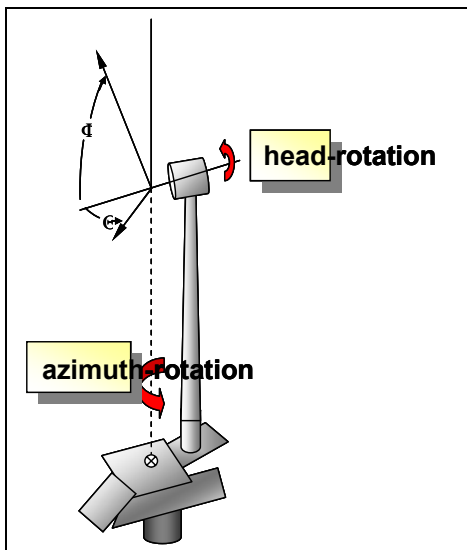


Figure 3. Antenna Test setting.

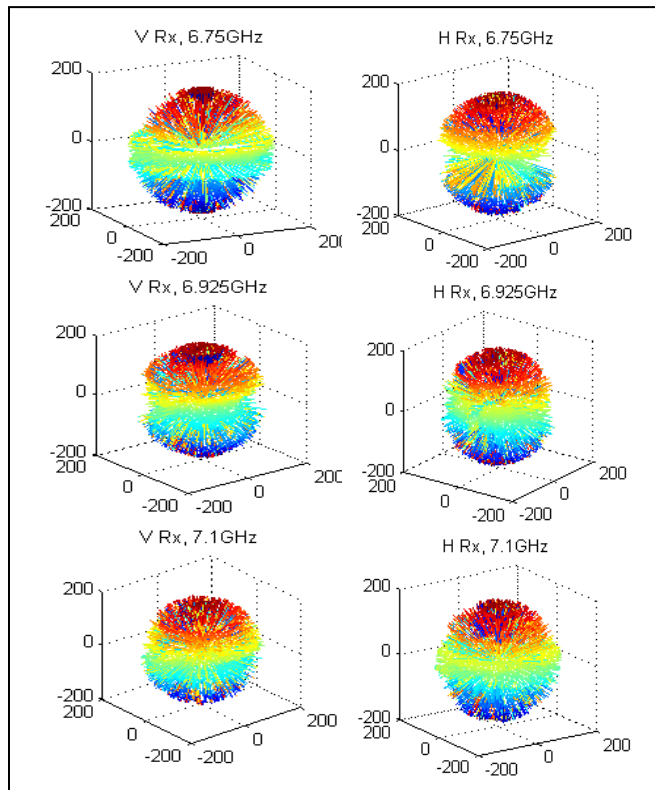


Figure 4. Differential phase between V and H pol as seen in 3D space.

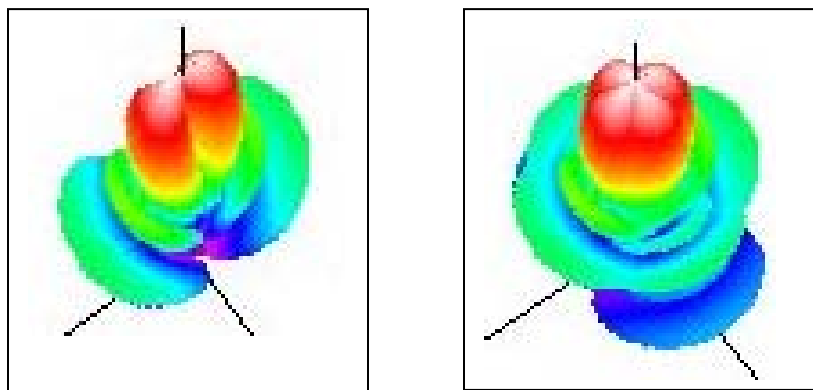


Figure 5. Left plot: 6.9 GHz ACMR H Tx Copol. Right plot: 6.9 GHz ACMR H Tx All pol.

The plots no longer exhibit overlapping problems.

(3) Input VSWR at the OMT ports (good) and VSWR variability as a function of distance to black body calibration box (excellent).

(4) Isolations between OMT ports (excellent)

(5) Transfer function for the module.

First, we considered the system {antenna+OMT +2 orthogonal polarization in free space} as a four-port network [5]. However, this approach seems uncertain when we deal with unguided wave at the input. Therefore, we chose to go back to the fundamental definitions as given in antenna radiation theory in order to link the input unguided fields to the output voltages at the OMT ports.

Suppose a dipole is fed by a 1A current, the field at the general receiving antenna is [6]:

$$\begin{cases} E_{\theta}^i = \frac{jZ_0}{2\lambda r} e^{-jkr} L_{\theta}, \\ E_{\phi}^i = \frac{jZ_0}{2\lambda r} e^{-jkr} L_{\phi}, \end{cases}$$

which can be rewritten: $\vec{E}^i = \frac{jZ_0}{2\lambda r} e^{-jkr} \vec{L}$,

where \vec{L} is the vector length of the dipole. By reciprocity, the voltage output at the receiving antenna is:

$$V = \frac{jZ_0}{2\lambda r} e^{-jkr} \vec{L} \cdot \vec{h} = \vec{E}^i \cdot \vec{h}(\theta, \phi).$$

Where \vec{E}^i is the impinging field on the antenna, and $\vec{h}(\theta, \phi)$ the effective length of the receiving antenna, equivalent to the pattern of that antenna in either receiving or transmitting mode. This effective length is the

same as in the well known expression of the transmitted field of a general antenna:

$$\vec{E}^o = \frac{jZ_0 I}{2\lambda r} e^{-jkr} \vec{h}(\theta, \phi).$$

Hence, for any scene emitting a field $\vec{E}^i = E_{\theta}^i \hat{u}_{\theta} + E_{\phi}^i \hat{u}_{\phi}$, the expected voltage outputs of the antenna are respectively for the V port and the H port:

$$\begin{cases} V_V = \iint_{\Omega_p} (h_{\theta}^V E_{\theta}^i + h_{\phi}^V E_{\phi}^i) d\Omega \\ V_H = \iint_{\Omega_p} (h_{\theta}^H E_{\theta}^i + h_{\phi}^H E_{\phi}^i) d\Omega \end{cases} \quad (1)$$

where

- $h_{\theta}^V(\theta, \phi)$ corresponds to ACMR pattern when the antenna is transmitting a V polarized wave and the Standard Feed Horn is receiving via its V port.
- $h_{\phi}^V(\theta, \phi)$ corresponds to ACMR pattern when the antenna is transmitting a V polarized wave and the Standard Feed Horn is receiving via its H port.
- $h_{\theta}^H(\theta, \phi)$ corresponds to ACMR pattern when the antenna is transmitting an H polarized wave and the Standard Feed Horn is receiving via its V port.
- $h_{\phi}^H(\theta, \phi)$ corresponds to ACMR pattern when the antenna is transmitting an H polarized wave and the Standard Feed Horn is receiving via its H port.

Expression (1) accounts for the antenna non idealities: phase delay at the antenna ports, mode leakage inside of the antenna, gain imbalance between the 2 ports.

As a first order approximation, we can consider that the observed scene is homogeneous, and that the antenna sidelobe and backlobe contributions are negligible compared to the main lobe of the antenna, plots of anechoic chamber measurements in

Figure 5 support this approximation. Therefore (1) can be simplified as follows:

$$\begin{cases} V_V = h_\theta^V E_\theta^i + h_\phi^V E_\phi^i \\ V_H = h_\theta^H E_\theta^i + h_\phi^H E_\phi^i \end{cases} \quad (2)$$

Open issues/Limitations

(1) Phase drift : no signal generator or VNA (receiver) phase lock and drift / phase noise information could be found. We noticed that, after a measurement protocol performance, a small phase drift had occurred. The measured phase is referenced to a fixed phase, regardless of what ACMR port is transmitting or when the measurements are performed. When antennas are facing boresight at the beginning of the protocol and at the end of the protocol, in a lapse of 4 hours, phase drift could be as large as 5 deg. It seems that technicians are confident that mechanical alignment before and after the protocol is not an issue.

(2) Nature of tapered range anechoic chamber not optimum for cross pol measurement:

- tests with CP antenna, shows creation of small cross pol when a supposed ideal copol is transmitted, amplitude can be tenths of dB to up to 0.5dB depending on the frequencies.
- rectangular chamber would be better, but no facilities at GSFC
- coaxial cables on AUT are asymmetric, Hport cable bents more than the Vport one.

(3) Further recommendations for next version of GAAMS.

Mainly, having the gain and phase referenced to the Device under Test would have saved some coding time. Also, being able to transmit both polarizations from the Antenna under test would lessen the risk of seeing phase drift since test protocol performance would take less time.

The Remote receiver and Polarimetric Circuit : Nature of the RRM and the PC and past contributions

The RRM and PC are shown respectively in Figures 6 and 7. The RRM ADC is now included in the computer and no longer ACMR. The PCM was also tested [2]. Summary of S parameters at 6.925GHz are given in Table 1.

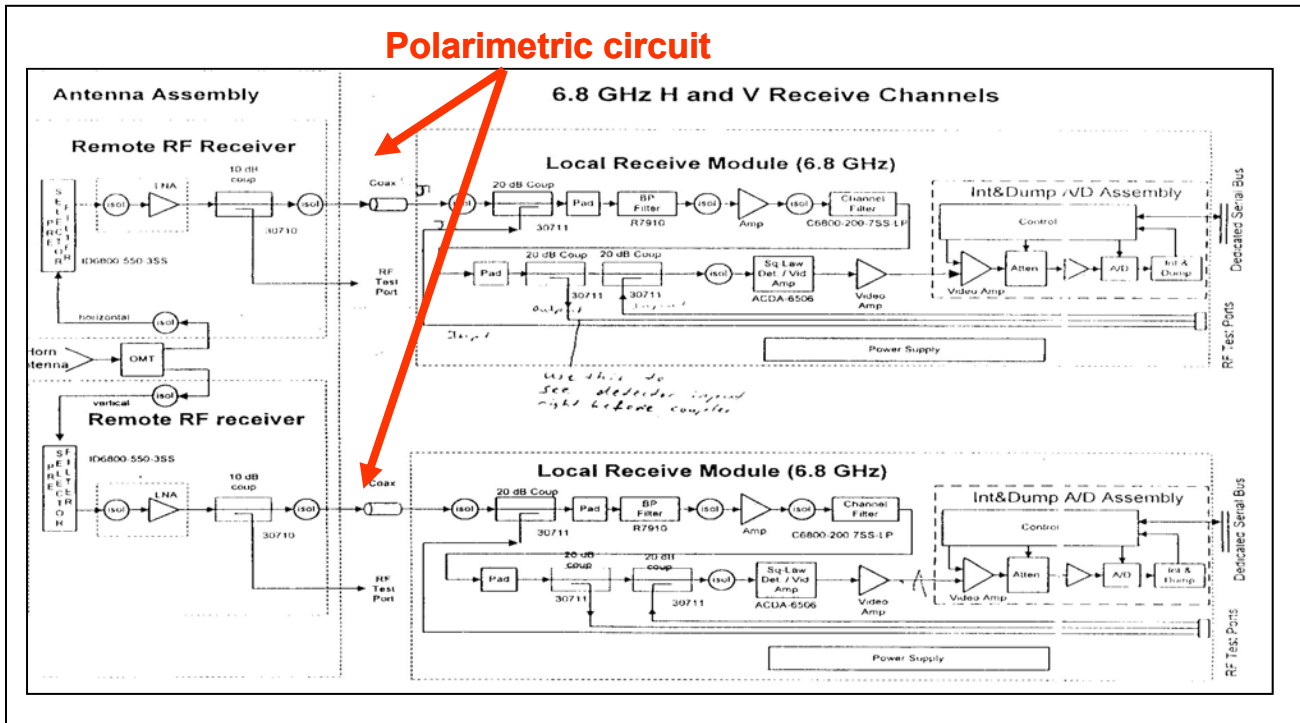


Figure 6. Remote Receiver Module

Table 1. Summary of S parameters of PC for 2 types of excitation

	SW1	SW2	SW3	SW4	SW5	SW6
V excite S11	~-27	~-15	~-24	~-24	~-25	~-24
V excite S21	~-5.517	~-9.474	~-9.292	~-12.917	~-12.802	~-60.183
V excite S12	~-5	~-9	~-9	~-13	~-13	~-62
V excite S22	~-22	~-18	~-24	~-30	~-19	~-25
H excite S11	~-18	~-17	~-18	~-17	~-19	~-20
H excite S21	~-59.821	~-9.645	~-9.749	~-9.256	~-9.37	~-5.554
H excite S12	~-60	~-10	~-10	~-9	~-9	~-5

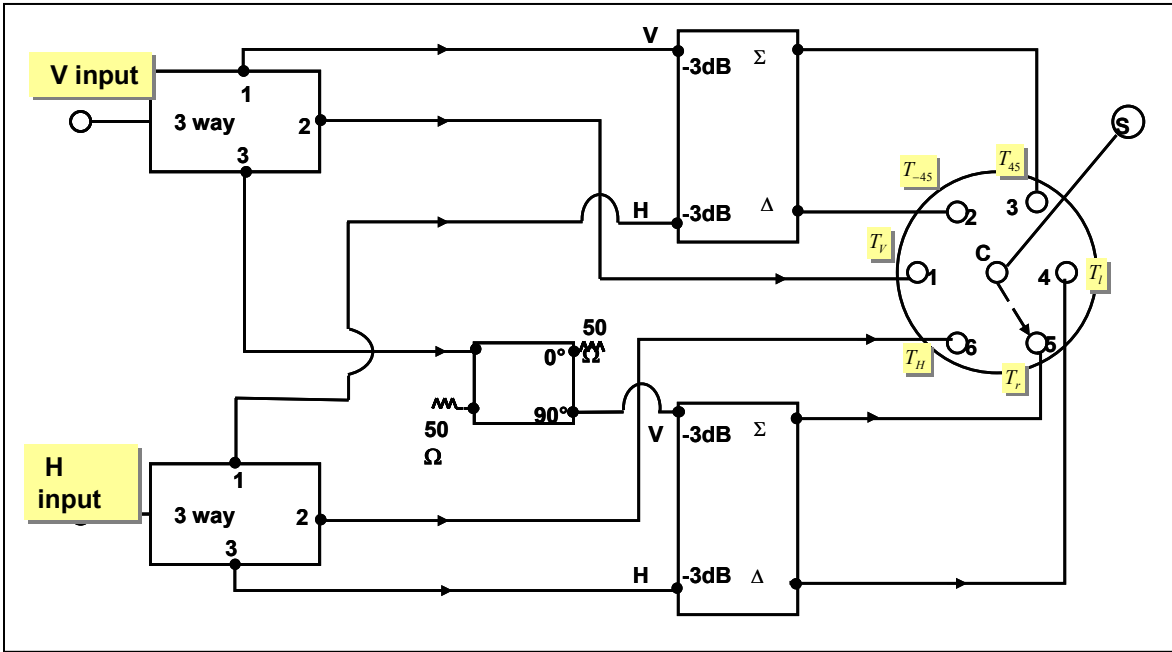


Figure 7. Polarimetric Circuit

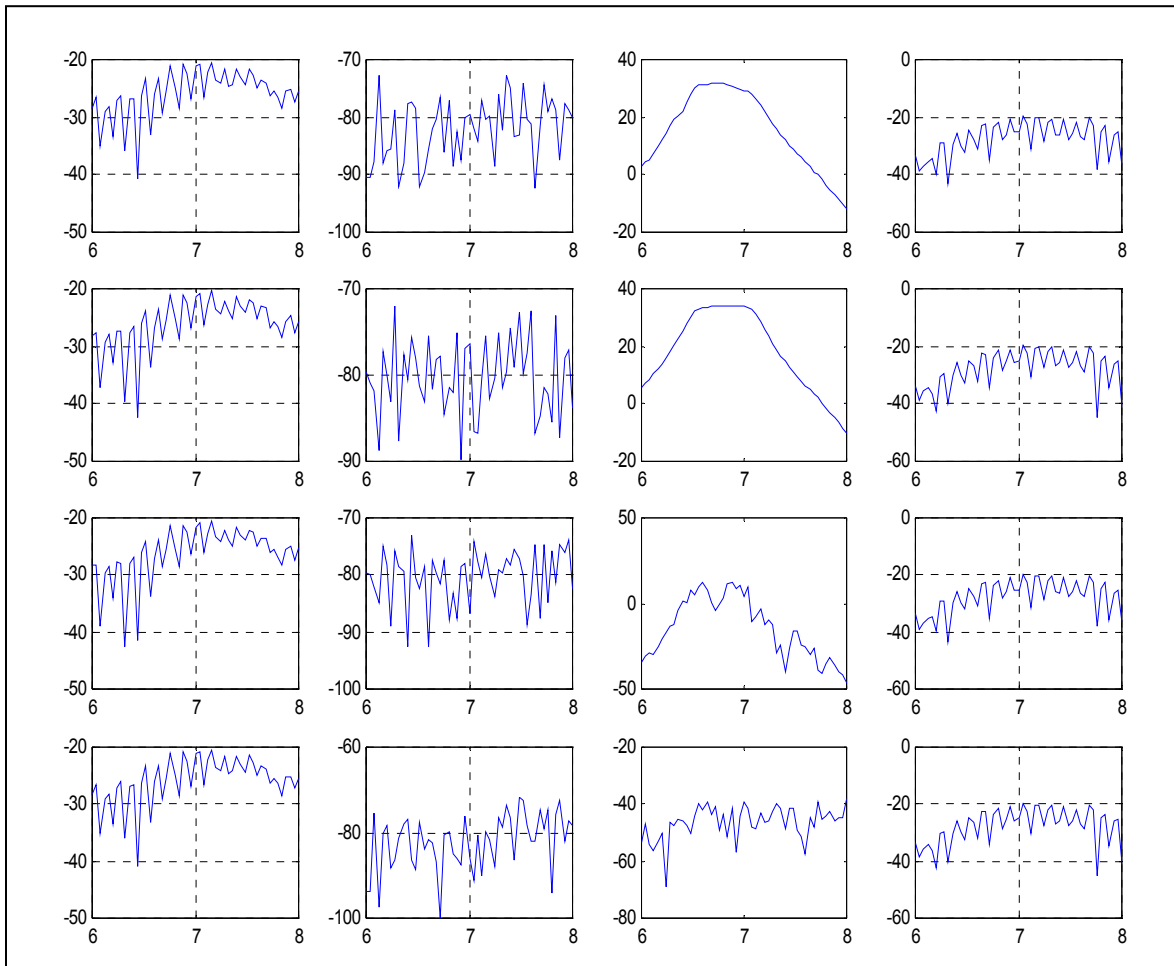


Figure 8. row: one file: VV/HH/HV/VH (port1port2)/column: each of the 4 part of a file: S11, S21, S12, S22. port 1: output of RR, port 2: input of RR

RESULTS

The RRM was tested with a Vector Network Analyzer HP8510 between 6 and 8 GHz in the following way: first, we considered the 2 port network consisting of the input V port and the output V port, second the 2 port network consisting of the input H port and the output H port. We also checked the isolation between the 2 input ports, between the 2 output ports. Finally, we measured the forward cross talk between the 2 channels. Figure 8 summarizes the obtained S parameters.

We are interested in deriving the transfer function of cascaded networks from the VNA measurements. Let us set the notations:

- a_i and b_i are the incoming and outgoing power waves in the classic microwave network theory.
- For the 4 port network RRM, the input V port, input H port, output V port and output H port are respectively noted port 1, 2, 3 and 4.
- Concerning the PCM, for each port excitation, and each switch position, a 2 port network model is adopted. Assuming superposition theory is applicable, we note $[S^a]$, $[S^b]$, $[S^c]$, $[S^d]$, $[S^e]$, and $[S^f]$ the scattering matrices for a V excitation and for the switch positioned at port 1, 2, 3, 4, 5 and 6 respectively. $[S^A]$, $[S^B]$, $[S^C]$, $[S^D]$, $[S^E]$, and $[S^F]$ corresponds to the same switch position for an H excitation.

Accordingly to the laboratory experimental results, 3 levels of approximation can be adopted depending on the wished level of calibration accuracy. Table 2 displays for each separate excitation port the models

adopted and the resulting transfer function via signal flow charts [8] for the combined RRM and PC.

The above approach, because of its analytical form, has the advantage to give some ideas about the weaknesses of the instrument and therefore to help engineers for future instrument designs.

The second order approximation seems to be a good trade-off between simplicity and accuracy. Using superposition, the output of the PC is the combination of the V and H excitations *at the input ports of the RRM*:

$$b_3'' = \frac{s_{21}^a s_{31} a_1'}{1 - \Gamma_l s_{22}^a} + \frac{s_{21}^A (s_{41} a_1' + s_{42} a_2')}{1 - \Gamma_l s_{22}^A} \quad (3)$$

Open issues/Limitations

The VNA tests of the cascaded system {RRM, PC} were carried out, and Ansoft Designer features the possibility to compute numerically the equivalent scattering matrix of that system. Future work includes comparisons between Ansoft designer simulations, measurements and analytical Mason's rule expressions.

Local Receiver Module/ ADC

The only measurement performed on the LRM was the measurement of the input VSWR, noted Γ_l in the previous section. Limitations to this measurement include the fact that the RF port is being square law detected therefore not terminated, which may account for the bad input VSWR, in the order of 0.35. No other sets of measurement were considered since for the LRM, the input is a RF one, and the output is a small voltage appearing on the computer screen.

Table 2. Different approximations for the cascaded system {RRM+PC}

For PCM V port excitation only			
	RRM model	PC model	Comment/Mason's rule
1 st order approximation	$\begin{bmatrix} b_1' \\ b_2' \\ b_3' \\ b_4' \end{bmatrix} = \begin{bmatrix} 0 & 0 & 0 & 0 \\ 0 & 0 & 0 & 0 \\ s_{31} & 0 & 0 & 0 \\ s_{41} & s_{42} & 0 & 0 \end{bmatrix} \begin{bmatrix} a_1' \\ a_2' \\ a_3' \\ a_4' \end{bmatrix}$	$\begin{bmatrix} b_1'' \\ b_3'' \end{bmatrix} = \begin{bmatrix} 0 & s_{12}^a \\ s_{21}^a & 0 \end{bmatrix} \begin{bmatrix} a_1'' \\ a_3'' \end{bmatrix}$	$b_3'' = s_{21}^a s_{31} a_1'$
2 nd order approximation	$\begin{bmatrix} b_1' \\ b_2' \\ b_3' \\ b_4' \end{bmatrix} = \begin{bmatrix} 0 & 0 & 0 & 0 \\ 0 & 0 & 0 & 0 \\ s_{31} & 0 & 0 & 0 \\ s_{41} & s_{42} & 0 & 0 \end{bmatrix} \begin{bmatrix} a_1' \\ a_2' \\ a_3' \\ a_4' \end{bmatrix}$	$\begin{bmatrix} b_1'' \\ b_3'' \end{bmatrix} = \begin{bmatrix} s_{11}^a & s_{12}^a \\ s_{21}^a & s_{22}^a \end{bmatrix} \begin{bmatrix} a_1'' \\ a_3'' \end{bmatrix}$	$b_3'' = \frac{s_{21}^a s_{31} a_1'}{1 - \Gamma_l s_{22}^a}$
3 rd order approximation	$\begin{bmatrix} b_1' \\ b_2' \\ b_3' \\ b_4' \end{bmatrix} = \begin{bmatrix} s_{11} & 0 & 0 & 0 \\ 0 & s_{22} & 0 & 0 \\ s_{31} & 0 & s_{33} & 0 \\ s_{41} & s_{42} & 0 & s_{44} \end{bmatrix} \begin{bmatrix} a_1' \\ a_2' \\ a_3' \\ a_4' \end{bmatrix}$	$\begin{bmatrix} b_1'' \\ b_3'' \end{bmatrix} = \begin{bmatrix} s_{11}^a & s_{12}^a \\ s_{21}^a & s_{22}^a \end{bmatrix} \begin{bmatrix} a_1'' \\ a_3'' \end{bmatrix}$	
	$\frac{b_3''}{a_1''} = \frac{s_{21}^a s_{31} (1 - \{s_{22} \Gamma_{s_2} + s_{44} \Gamma_{l_4}\} + \{s_{22} \Gamma_{s_2} s_{44} \Gamma_{l_4}\})}{1 - \sum L(1) + \sum L(2) - \sum L(3) + \sum L(4) - \sum L(5)}$		
For PCM H port excitation only			
1 st order approximation	$\begin{bmatrix} b_1' \\ b_2' \\ b_3' \\ b_4' \end{bmatrix} = \begin{bmatrix} 0 & 0 & 0 & 0 \\ 0 & 0 & 0 & 0 \\ s_{31} & 0 & 0 & 0 \\ s_{41} & s_{42} & 0 & 0 \end{bmatrix} \begin{bmatrix} a_1' \\ a_2' \\ a_3' \\ a_4' \end{bmatrix}$	$\begin{bmatrix} b_2'' \\ b_3'' \end{bmatrix} = \begin{bmatrix} 0 & s_{12}^A \\ s_{21}^A & 0 \end{bmatrix} \begin{bmatrix} a_2'' \\ a_3'' \end{bmatrix}$	$b_3'' = s_{21}^A s_{41} a_1' + s_{21}^A s_{42} a_2'$
2 nd order approximation	$\begin{bmatrix} b_1' \\ b_2' \\ b_3' \\ b_4' \end{bmatrix} = \begin{bmatrix} 0 & 0 & 0 & 0 \\ 0 & 0 & 0 & 0 \\ s_{31} & 0 & 0 & 0 \\ s_{41} & s_{42} & 0 & 0 \end{bmatrix} \begin{bmatrix} a_1' \\ a_2' \\ a_3' \\ a_4' \end{bmatrix}$	$\begin{bmatrix} b_2'' \\ b_3'' \end{bmatrix} = \begin{bmatrix} s_{11}^A & s_{12}^A \\ s_{21}^A & s_{22}^A \end{bmatrix} \begin{bmatrix} a_2'' \\ a_3'' \end{bmatrix}$	$b_3'' = \frac{s_{21}^A (s_{41} a_1' + s_{42} a_2')}{1 - \Gamma_l s_{22}^A}$
3 rd order approximation	$\begin{bmatrix} b_1' \\ b_2' \\ b_3' \\ b_4' \end{bmatrix} = \begin{bmatrix} s_{11} & 0 & 0 & 0 \\ 0 & s_{22} & 0 & 0 \\ s_{31} & 0 & s_{33} & 0 \\ s_{41} & s_{42} & 0 & s_{44} \end{bmatrix} \begin{bmatrix} a_1' \\ a_2' \\ a_3' \\ a_4' \end{bmatrix}$	$\begin{bmatrix} b_2'' \\ b_3'' \end{bmatrix} = \begin{bmatrix} s_{11}^A & s_{12}^A \\ s_{21}^A & s_{22}^A \end{bmatrix} \begin{bmatrix} a_2'' \\ a_3'' \end{bmatrix}$	
	$\frac{b_3''}{(s_{41} a_1' + s_{42} a_2')} = \frac{s_{21}^A s_{31} (1 - \{s_{33} \Gamma_l + s_{22} \Gamma_{s_2}\} + \{s_{33} \Gamma_l s_{22} \Gamma_{s_2}\})}{1 - \sum L(1) + \sum L(2) - \sum L(3) + \sum L(4) - \sum L(5)}$		

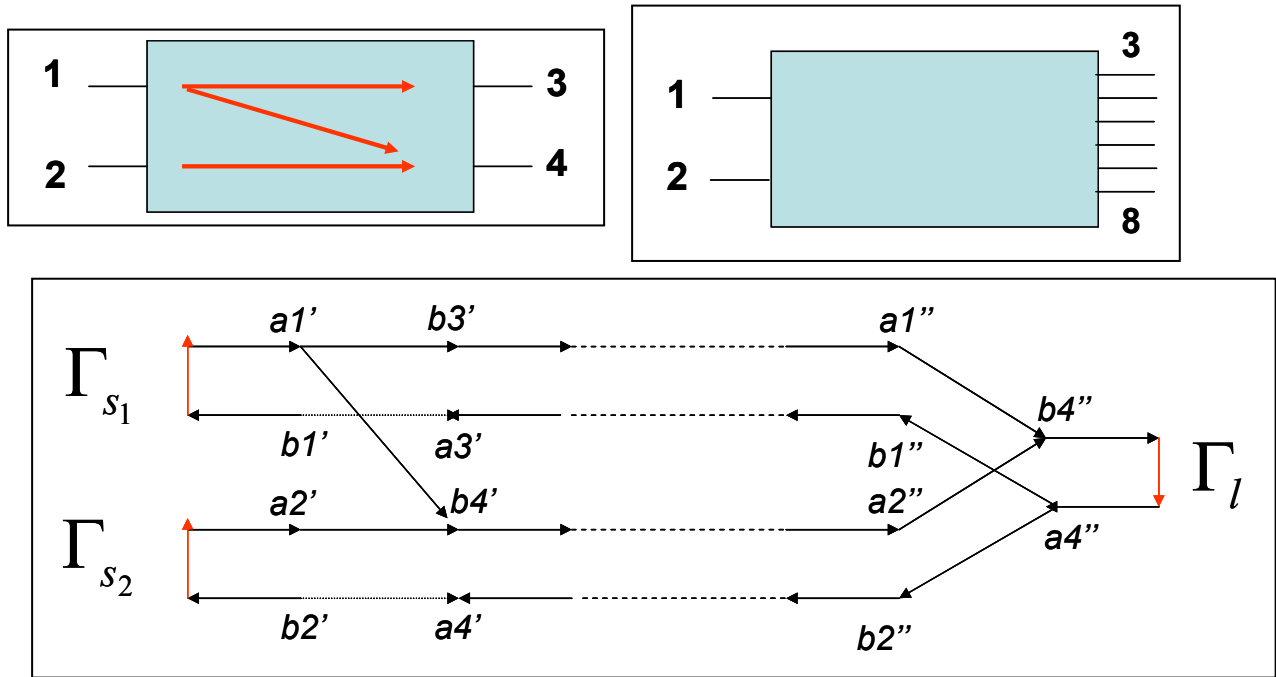


Figure 9. Cascaded microwave networks {RRM+PC} and corresponding signal flow diagrams

Transfer function

Let us derive the relationship between the input modified Stokes parameters and the output voltages.

Inserting (2) into (3):

$$b_3'' = \left\{ \left(\frac{S_{21}^a S_{31}}{1 - \Gamma_l S_{22}^a} + \frac{S_{21}^A S_{41}}{1 - \Gamma_l S_{22}^A} \right) h_\theta^V + \left(\frac{S_{21}^A S_{42}}{1 - \Gamma_l S_{22}^A} \right) h_\theta^H \right\} E_V + \left\{ \left(\frac{S_{21}^a S_{31}}{1 - \Gamma_l S_{22}^a} + \frac{S_{21}^A S_{41}}{1 - \Gamma_l S_{22}^A} \right) h_\phi^V + \left(\frac{S_{21}^A S_{42}}{1 - \Gamma_l S_{22}^A} \right) h_\phi^H \right\} E_H$$

can be written as: $b_3'' = A_3 E_V + B_3 E_H$

Let us use complex expressions: $\begin{cases} A_3 = |A_3| e^{j\alpha_3} \\ B_3 = |B_3| e^{j\beta_3} \end{cases}$

Also, let us consider that: $\begin{cases} E_V = E_v \cos(\omega t) \\ E_H = E_H \cos(\omega t - \delta) \end{cases}$. Hence, $\begin{cases} E_V = |E_V| \\ E_H = |E_H| e^{-j\delta} \end{cases}$

Suppose the signal is being amplified by a gain G_{23} , it is then square law detected and the user has access to an average of that number, hence:

$$\langle v_{out_3} \rangle = \langle |G_{23} b_3|^2 \rangle = \langle |G_{23}|^2 \{ |A_3|^2 |E_V|^2 + |B_3|^2 |E_H|^2 + 2 \operatorname{Re}(A_3 \|E_V\| B_3 \|E_H\| e^{j(\alpha_3 - \beta_3 + \delta)}) \} \rangle$$

Assume G_{23} , A_3 and B_3 are time independent, because they describe parts of the system that are stable in time since thermal control is enforced. Using linearity of the operator $\langle \dots \rangle = \frac{1}{T} \int_0^T \dots dt$, we obtain:

$$\langle v_{out_3} \rangle = |G_{23}|^2 \{ |A_3|^2 \langle |E_V|^2 \rangle + |B_3|^2 \langle |E_H|^2 \rangle + 2 |A_3| \|E_V\| |B_3| \|E_H\| \langle \cos(\alpha_3 - \beta_3 + \delta) \rangle \}$$

Let us assume that: $|E_V|$, $|E_H|$ and δ are time independent.

Posing $C = \frac{\lambda^2}{k_B \eta}$ and noticing that:

$$\left\{ \begin{array}{l} \langle |E_V|^2 \rangle = \frac{T_V}{C} \\ \langle |E_H|^2 \rangle = \frac{T_H}{C} \\ 2 |E_V| \|E_H\| \cos(\delta) = \frac{T_3}{C} \\ 2 |E_V| \|E_H\| \sin(\delta) = \frac{T_4}{C} \end{array} \right.$$

we derive the expression of the output voltage for a noisefree system:

$$\langle v_{out_3} \rangle = \frac{|G_{23}|^2}{C} \{ |A_3|^2 T_V + |B_3|^2 T_H + |A_3| |B_3| (\cos(\alpha_3 - \beta_3) T_3 - \sin(\alpha_3 - \beta_3) T_4) \}$$

The real system is equivalent to the noisefree system described above, receiving the emission from the scene and noise as shown in Figure 10.

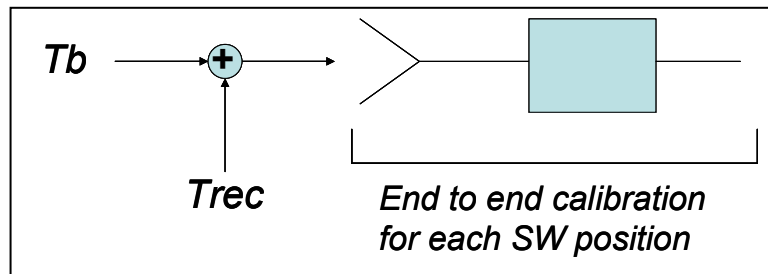


Figure 10. Real system including Trec at the input

Thus, the equivalent receiver noise temperature enters the system in the V and H channels. 3rd and 4th Stokes parameters also have noise contributions via the difference of equivalent noise temperature between switch position 5 and 4, and 6 and 7 respectively.

Generalizing for the other PC switch positions, we obtain the overall description of ACMR linking the output voltages to the modified Stokes vector of the scene under observation:

$$\begin{pmatrix} \langle V_{out3} \rangle \\ \langle V_{out4} \rangle \\ \langle V_{out5} \rangle \\ \langle V_{out6} \rangle \\ \langle V_{out7} \rangle \\ \langle V_{out8} \rangle \end{pmatrix} = \frac{1}{C} \begin{bmatrix} |G_{23}|^2 \\ |G_{24}|^2 \\ |G_{25}|^2 \\ |G_{26}|^2 \\ |G_{27}|^2 \\ |G_{28}|^2 \end{bmatrix} \mathbf{0} \begin{bmatrix} |A_3|^2 & |B_3|^2 & |A_3||B_3|\cos(\alpha_3 - \beta_3) & -|A_3||B_3|\sin(\alpha_3 - \beta_3) \\ \dots & \dots & \dots & \dots \\ |A_8|^2 & |B_8|^2 & |A_8||B_8|\cos(\alpha_8 - \beta_8) & -|A_8||B_8|\sin(\alpha_8 - \beta_8) \end{bmatrix} \begin{bmatrix} T_V - T_{rec3} \\ T_H - T_{rec8} \\ T_3 - (T_{rec5} - T_{rec4}) \\ T_4 - (T_{rec6} - T_{rec7}) \end{bmatrix}$$

We will refer to this expression to the *radiometer transfer function* or Jones matrix [7].

Table 3.

	Switch position	1	2	3	4	5	6
Cold target	V mean (V)	0.089755	0.096721	0.099953	0.078943	0.083133	0.154882
	V std dev (V)	3.56e-5	2.78e-5	2.98e-5	1.91e-5	1.86e-5	2.92e-5
Ambient target	V mean (V)	0.147665	0.159151	0.164768	0.130976	0.137923	0.253816
	V std dev (V)	3.45e-05	2.88e-5	2.18e-5	2.07e-5	2.11e-5	3.57e-5

Table 4.

Switch position	1	2	3	4	5	6
Gain (V/K)	2.597e-4	2.8e-4	2.906e-4	2.333e-4	2.457e-4	4.436e-4
-Trec	-268.6279	-268.4893	-266.8973	-261.3321	-261.3616	-272.1099

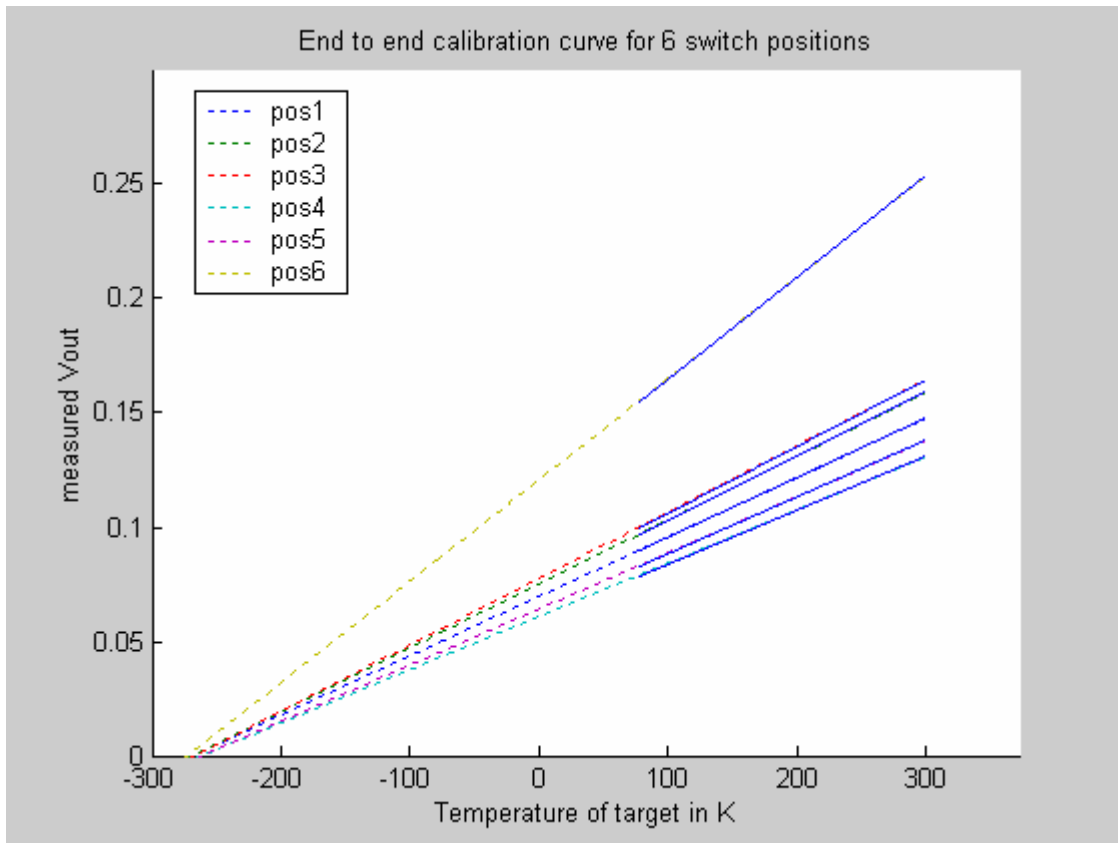


Figure 11: Laboratory end to end calibration

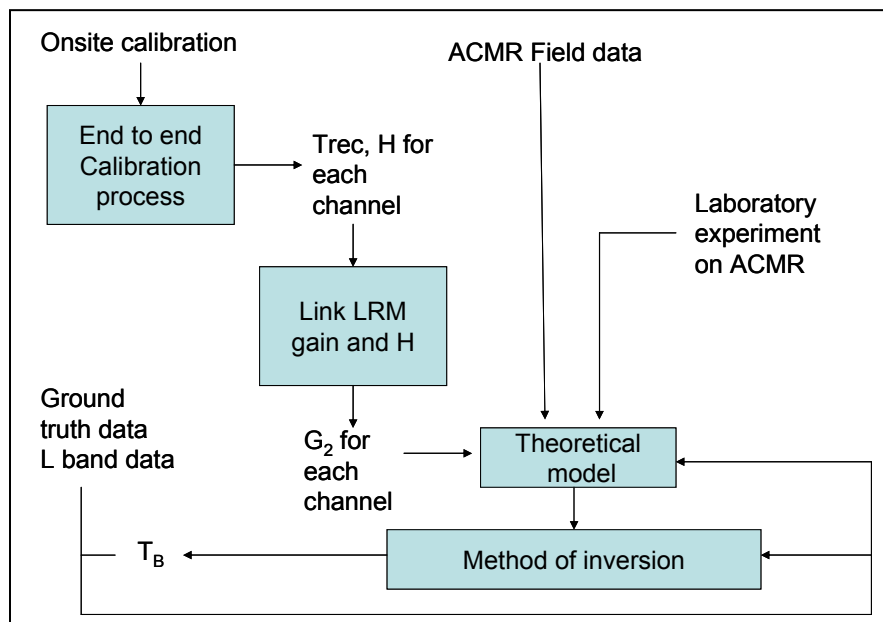


Figure 12: Process for Stokes vector retrieval

Temperature calibration/ gain measurement. : End to end system characterization

Previous work included only the end to end characterization for one switch position. Since the signal goes through different paths depending on the switch position, we decide to perform an end to end calibration of the radiometer for each one of the six switch positions. The antenna pointed at an unpolarized absorber target at ambient temperature (27°C) or at liquid nitrogen temperature (77K). The output voltages corresponding to the 6 different switch positions and 30s dwelling time were recorded. Only voltage means presenting a standard deviation on the order of 10^{-4} were kept as shown in Table 3. With these two points, end to end calibration curves for each on of the switch position were obtained in Figure 11.

Using a linear interpolation, we obtain for each one of the switch position, equivalent

independent radiometer gains and receiver noise temperature T_{rec} , as displayed in Table 4. Thus, on average the equivalent noise temperature is 266.4797K for a standard deviation of 4.3178K, eg 1.62%. Therefore as a first order approximation, we will consider that the equivalent noise temperature is the same for all switch positions.

Field data : Rebex7

The Radiobrightness and Energy Balance Experiment 7 was held in Michigan in October 2000 with senescent corn [9]. End to end calibration used sky and absorber box at ambient temperature. Also, ground truth data is available.

For October, 10th 2000 in the morning, the following receiver equivalent noise temperatures are obtained with a post protocol sky and absorber calibration.

T_{rec}	260.8068	290.9588	271.6273	285.2358	270.3952	296.5281
-----------	----------	----------	----------	----------	----------	----------

Plain calibration yields the plot in Figure 13 for different arm positions for V and H pol:

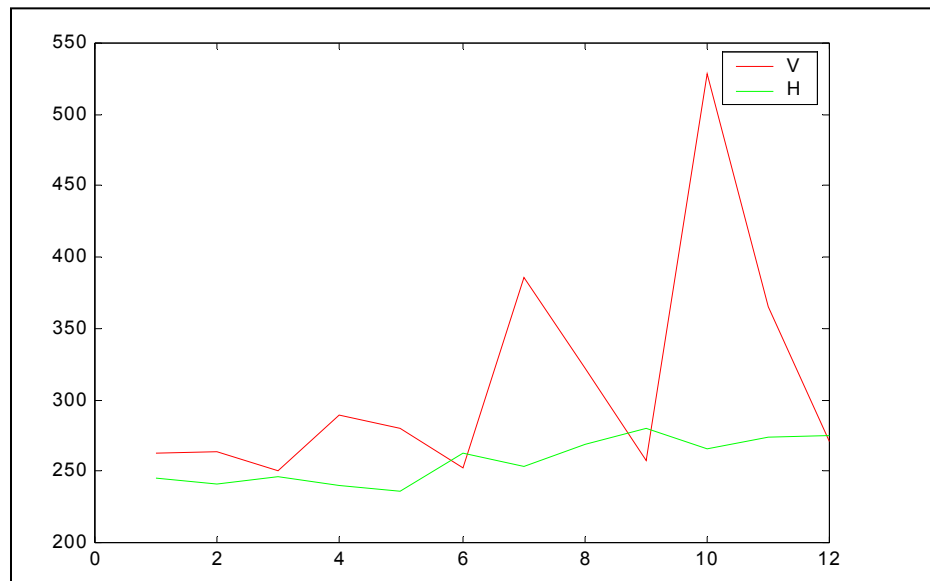


Figure 13: Plain calibration

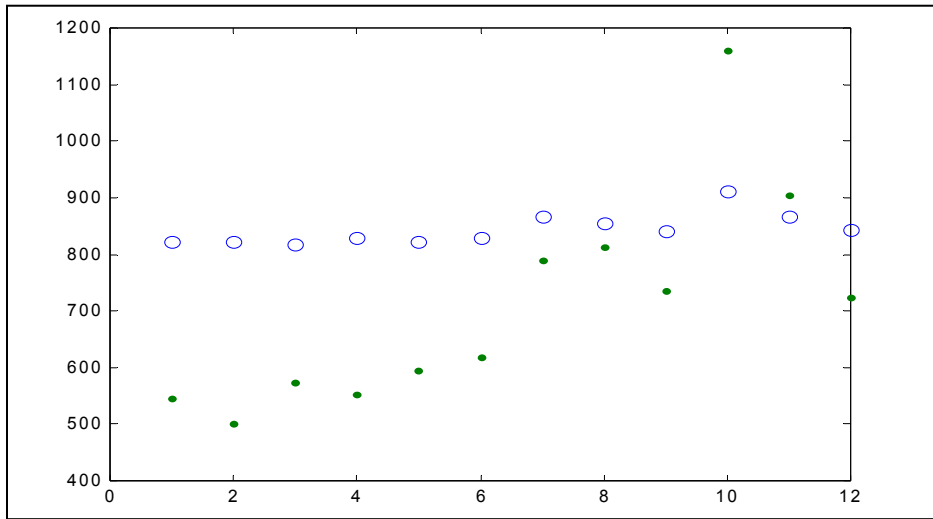


Figure 14. Same trends when using 6 by 2 Jones matrix

If we use a 6 by 4 Jones matrix, we get the same trends for V and H, but the scaling problem has gotten worse. We notice that 3rd and 4th Stokes parameters have different behaviors. (Figure 15)

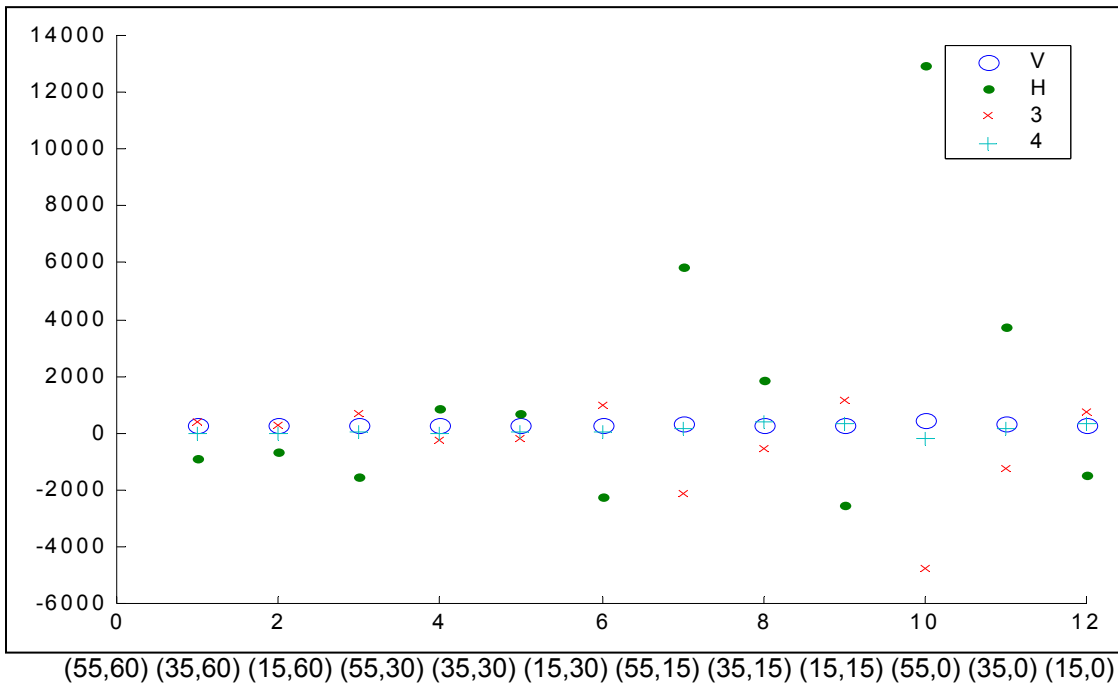


Figure 15. Obtention of Stokes parameters trends with scaling problem.

CONCLUSION

Contribution for this summer work included:

- extensive laboratory measurements of ACMR
- theoretical model describing non-idealities
- 1st order retrieval of REBEX7 full modified Stokes vector

There is a high level of confidence as to the obtained trends for the 4 Stokes parameters, nevertheless there is obviously a scaling problem. Temporal coherence was investigated and path lengths of the system shouldn't be an issue.

Future calibration work will include:

- Comparison with Ansoft Designer numerical results
- Refinement study to obtain absolute temperatures
- Quantitative error analysis
- Investigation of inversion sensitivity
- Feedback for future instrument design.

In order to better condition the system, it may be useful to express the 6 PC output as a function of 6 input brightness temperatures, indeed there is no real possibilities to select only 4 equations out of 6, because of the interdependence between the channels.

REFERENCES

- [1] Ulaby et Al, RS : Passive and active, Artech, 1982
- [2] A. Imig, Summer internship report, 2001.
- [3] H. Pham, ACMR antenna test procedure report, 2003
- [4] A. C. Ludwig, The definition of Cross-polarization, IEEE TAP, Vol. 21, pp 116-119, Jan.1973
- [5] W. L. Stutzman, Polarization in electromagnetic systems, Artech house, 1993
- [6] H. Mott, Antennas for radar and communications, a polarimetric approach, Wiley series microwave and optical engineering (1992)
- [7] J.P. Hamaker et al, « Understanding radio polarimetry (I) », Astronomy & astrophysics supplement series. 117, 137-147 (1996)
- [8] D. M. Pozar, Microwave engineering, Addison-Wesley (1990)
- [9] B. K. Hornbuckle, Report on REBEX7, 2000